Materials & Design 219 (2022) 110799

Contents lists available at ScienceDirect

Materials & Design

journal homepage: www.elsevier.com/locate/matdes

Processing time, temperature, and initial chemical composition prediction from materials microstructure by deep network for multiple inputs and fused data

Amir Abbas Kazemzadeh Farizhandi [a], Mahmood Mamivand [b,*]

[a] Computer Science Department, Boise State University, United States
[b] Department of Mechanical and Biomedical Engineering, Boise State University, United States

HIGHLIGHTS

- The possibility of inverse design in material design by artificial intelligence has been demonstrated.
- The chemical composition and processing history were predicted from materials microstructure morphology.
- A fused-data deep learning framework has been trained to predict the chemical compositions, temperature and time processing of a microstructure.
- The error analysis shows that the majority of the wrong predictions are indeed not wrong, but the other right answers.
- The trained network was successfully validated with an experimental Fe-Cr-Co transmission electron microscopy micrograph.

GRAPHICAL ABSTRACT

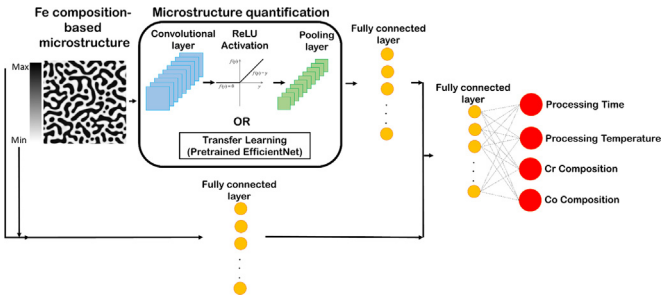

ARTICLE INFO

Article history:
Received 4 April 2022
Revised 13 May 2022
Accepted 28 May 2022
Available online 4 June 2022

Keywords:
Microstructure-mediated materials design
Process history prediction
Deep learning
Transfer learning
Materials informatics

ABSTRACT

Prediction of the chemical composition and processing history from microstructure morphology can help in material inverse design. In this work, we propose a fused-data deep learning framework that can predict the processing history of a microstructure. We used the Fe-Cr-Co alloys as a model material. The developed framework is able to predict the heat treatment time, temperature, and initial chemical compositions by reading the morphology of Fe distribution and its concentration. The results show that the trained deep neural network has the highest accuracy for chemistry and then time and temperature. We identified two scenarios for inaccurate predictions; 1) There are several paths for an identical microstructure, 2) Microstructures reach steady-state morphologies after a long time of aging. The error analysis shows that the majority of the wrong predictions are indeed not wrong, but the other right answers. We validated the model successfully with an experimental Fe-Cr-Co transmission electron microscopy micrograph.

* Corresponding author.
E-mail address: mahmoodmamivand@boisestate.edu (M. Mamivand).

https://doi.org/10.1016/j.matdes.2022.110799
0264-1275/

1. Introduction

Accelerating the speed of materials development and discovery has been the focus of intensive research in the last two decades, in particular after the lunch of the US Materials Genome Initiative [1-6]. In this regard, multi-scale modeling and simulation along with limited informed experiments, have been identified as key factors, as they can significantly reduce the time and effort required for high throughput exploration in materials space [7-11]. However, in the meantime, there is growing recognition that simulations alone will not provide the desired acceleration in materials development. Developing and deploying an appropriate support data infrastructure that efficiently integrates closed-loop iterations between experimentation and multi-scale modeling/simulation efforts is climacteric. This need is addressed by a new interdisciplinary field called Materials Data Science and Informatics [12-18].

A fundamental element of the data science approach is a multi-faceted framework that enables the research community to collect, aggregate, nurture, disseminate, and reuse valuable knowledge. In materials innovation efforts, this knowledge is primarily desired in the form of length and time scale process-structure–property (PSP) linkages associated with the material system of interest [19-24]. In a multi-scale materials modeling effort, this means developing a formal data science approach to extract reusable PSP linkages from an ensemble of simulation and experiment datasets, as depicted in Fig. 1. The top arrow in Fig. 1, forward design philosophy, shows a typical workflow that materials scientists historically have used in developing PSP linkages. In forward design philosophy, we loop through the ordered connection of process-structure-property. Forward design usually involves the use of experiments and advanced physics in combination with numerical algorithms. Generally, since material discovery requires exploration of big space, the forward design is prone to result in high costs and time. This cost can be a significant obstacle to materials innovation efforts, even in the realm of simulations, as these simulations are often expensive and the design space is huge. This is precisely where the data science approaches offer many benefits. As shown in Fig. 1, the data science tools and algorithms can enable us to perform inverse design, i.e., start from the desired properties and find the required processing. The data science with taking full advantage of advanced statistics and machine learning techniques can provide a mathematically rigorous framework for PSP linkage in multi-scale material design. As depicted in Fig. 1, one of the main benefits of adding data science components to the entire workflow is that it is very practical to solve the inverse problem, which is the ultimate goal of materials innovation efforts. In fact, materials informatics provides a low computational approach for materials design. This is mainly because the PSP linkages are cast as meta-models or surrogate models. These models can be easily used to find the optimum conditions for making materials with desired properties.

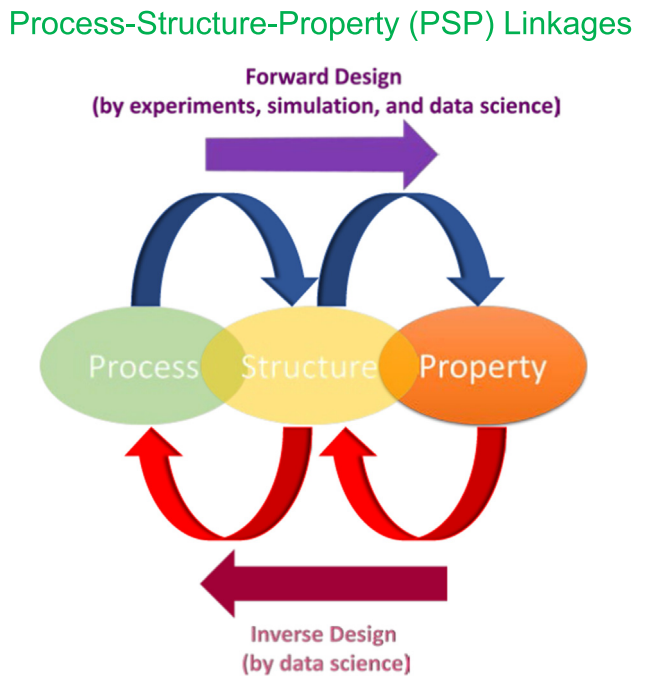

Fig. 1. Schematic of materials design workflow by forward and inverse design using PSP linkages.

Artificial intelligence (AI), machine learning (ML), and data science can help speed up and simplify the process of discovering new materials [25]. In recent years, the use of data science in various areas of materials science has increased significantly [26-31]. For example, data science is applied to assist in calculating density functional theory and to correlate atomic interactions with materials properties based on quantum mechanics [32-35]. AI is also used to create PSP linkages in the context of the materials design. In this case, one can use ML to design new materials with the desired properties or optimize the existing materials' manufacturing processes to improve their properties. Researchers can study/identify the complex and non-linear link between the materials manufacturing processes and properties through data science. For instance, in the context of forward design, several works attempted to predict the materials' structure from the process parameters or the material properties from the microstructure and manufacturing history [26,36-44].

The main obstacle in implementing the (micro)structure → pro cess → chemistry approach is the lack of a validated and widely accepted framework for rigorously quantifying hierarchical materials microstructures. The microstructure plays a central role in forming the PSP linkages and is often a vital input and output. In addition, microstructures often require a higher dimensional representation compared to other variables related to PSP linkages. From a practical point of view, it is essential to find suitable low-dimensional representations for the materials' microstructure to be able to use them in PSP linkages construction. While this is a crucial factor in developing a high-quality, reusable materials knowledge system [45], traditionally, this dimensionality reduction has been carried out by materials scientists based on intuition or insight into the material phenomenon being studied. As a concrete example, when looking at plastic responses, particle size or shape distributions and possibly orientation and misalignment distributions can be used to quantify polycrystalline microstructures [46]. However, such an approach has not yet identified a broad set of low-dimensional metrics that can be universally applied to different materials systems to identify most materials' properties.

In recent years, deep learning (DL) techniques have been successfully used in the areas such as computer vision. Their recent use in materials science has also proved to be a reliable and promising method [39]. The main advantages of the DL method are its simplicity, flexibility, and applicability to all types of materials structures. All these advantages increased the application of DL in materials science noticeably [35,40-44,47-49]. One form of DL model that is widely used for feature extraction in various applications such as image, video, audio, and natural language processing is a convolutional neural network (CNN) [50-53]. In materials science, CNN has been used for various image-related problems [54]. Cang et al. [54] used CNN to achieve a dimensionality reduction of 1/1000 from the microstructure space. In DeCost et al. [55] work, CNN was applied to microstructure segmentation. Xie and Grossman [56] used CNN to quantify crystal diagrams and

predict materials' properties, including accurately predicting eight different material properties such as formation energy, bandgap, and shear modulus. CNNs were also used to index electron backscatter diffraction patterns and determine the crystal orientation of crystalline materials [57]. Yang et al. [58] predicted the stiffness of two-phase composites by deep learning approaches that included both convolutions and fully-connected layers. Also, in comparison to the other microstructural quantification techniques, such as the n-point correlation methods, the features extracted by CNN can provide more accurate predictions [20,59-64].

One drawback of deep CNN is the need for a large training dataset, which is not always available in many applications. To alleviate this problem, feature extraction can be performed by transfer learning methods using the pre-trained networks. Though pre-trained networks have been trained by non-domain specific image databases, such ImageNet [65], it has been shown that transfer learning can be useful, especially in materials science, where image-based data is generally not very abundant. DeCost et al. [66] used the pre-trained VGG16 to classify the steel microstructures based on the annealing conditions. VGG16 was also applied to extract and classify the features from scanning electron microscope (SEM) images [26]. Lubbers et al. [67] adopted the VGG19 to identify the physically important descriptors within the microstructures. VGG19 has also been used to develop a framework for materials structure reconstruction and property prediction [68].

The above overview shows that the majority of ML microstructure-related works in the materials science community have been focused on microstructure classification [69-71], detection [72], and reconstruction [68,73] or finding a relationship between materials morphologies and properties [37,58,74]. However, the process and chemistry predictions from microstructure morphology images have received limited attention. This is an important knowledge gap for considerable materials systems that we have some knowledge on the ideal morphologies, either from theories or simulations. However, the chemistry and processing routes that guide us to the goal morphology are not known. A critical challenge to address this knowledge gap is the inverse design based on the microstructure morphology. This design especially gets more challenging for multi-component/multi-phase materials. Recently, Kautz et al. [37] have used the CNN for microstructure classification and segmentation of uranium alloyed with 10 wt% molybdenum (U-10Mo). They used a segmentation algorithm to calculate the area fraction of the lamellar transformation product of αU + γUMo and inserted the total area fraction into the Johnson-Mehl-Avrami-Kolmogorov equation to predict the annealing parameters. Some limitations of their work are the missing information about the morphology and particle distribution and the absence of chemistry for aging time prediction.

In our prior work [75], we proposed a framework based on deep learning to predict the process parameters and chemical compositions from materials micrographs in a steady-state condition. Therefore, the developed model did not have the processing time as an important processing parameter. Consequently, the materials' microstructure evolution over time was missing. In this study, we will propose a model based on a deep neural network to predict a complete set of processing parameters, including temperature, time, and chemistry from a microstructure micrograph. As a case study, we focused on the spinodal decomposition process, and to prove the model applicability for realistic alloys, we picked the Fe-Cr-Co permanent magnets as the model alloy. We used the phase-field (PF) method to create the training and test datasets for the deep network training. A fused dataset including material microstructure as well as minimum and maximum iron concentration in the microstructure is used as the input data. We quantified the generated microstructures with the CNN and then combined the extracted salient features from the microstructures with iron composition to predict the processing history, i.e., annealing time and temperature, and chemical compositions of the micrograph.

2. Methods

2.1. Phase-field modeling

In this study, we used the phase-field (PF) method to generate the training and test dataset. In the past two decades, the PF method has gained considerable attention as a powerful tool for simulating a wide range of moving boundary problems, including solidification, solid-state phase transformation, crack growth, etc [76]. To simulate the process of phase separation in Fe-Cr-Co alloy we have used the standard PF model for conserved parameters, i.e., the Cahn-Hilliard (CH) equations. Since the diffusion of constituent elements controls the process of phase separation, the PF parameters in this study are the concentration of Fe, Cr, and Co. Therefore, the governing equations for Fe-Cr-Co spinodal decomposition are,

$$\frac{\partial c_{Cr}}{\partial t} = \nabla \cdot M_{Cr,Cr} \nabla \frac{\delta F_{tot}}{\delta c_{Cr}} + \nabla \cdot M_{Cr,Co} \nabla \frac{\delta F_{tot}}{\delta c_{Co}} \quad (1)$$

$$\frac{\partial c_{Co}}{\partial t} = \nabla \cdot M_{Co,Cr} \nabla \frac{\delta F_{tot}}{\delta c_{Cr}} + \nabla \cdot M_{Co,Co} \nabla \frac{\delta F_{tot}}{\delta c_{Co}} \quad (2)$$

where c_{cr} and c_{co} are concentrations of Chromium and Cobalt, t is time, F_{tot} is total free energy, and M is mobility function. The microstructure evolution is primarily driven by the minimization of the total free energy F_{tot} of the system. We parametrized the model with the calculation of phase diagram (CALPHAD) data [77]. To solve the non-linear CH partial differential equations (PDEs), we used the Multi-physics Object-Oriented Simulation Environment (MOOSE). MOOSE is an open-source finite element package developed at Idaho National Laboratory and efficient for parallel computation on supercomputers [78]. The coupled CH equations were solved with the help of MOOSE's prebuilt series of weak form residuals of CH PDEs with the input parameters given in Table S1 in Supplementary Materials.

2.2. Training and test dataset

The goal of the presented work in this study is to develop a framework that is able to predict the processing history and chemistry of a micrograph just by reading one element's morphological distribution. For the specific case study of spinodal decomposition in this work, the processing parameters are annealing temperature and time. Therefore, to develop proper training and test datasets, we need to span the possible ranges of input variables, i.e., time, temperature, and chemical compositions. For the temperature, we are bonded to the range of 850–970 K, as spinodal decomposition in Fe-Cr-Co happens in this window. For chemistry, we explore the range of 0.05–0.9 at. % for both Cr and Co. Since the chemistry is subjected to the conservation of mass constrain, i.e., $c_{Fe} + c_{Cr} + c_{Co} = 1$, we used the Simplex-Lattice [79] as a mixture design method to generate the chemistry space to explore. Finally, we bounded the dataset to 300 h for the time, as our study showed most microstructures would reach equilibrium to some extent by this time. Unlike temperature and chemistry, we did not grid the time domain linearly because the microstructure is very sensitive to aging time in the early stages of annealing, but this sensitivity drops dramatically as time passes. Therefore, we picked a fine grid at the beginning, 50 s, and increased it exponentially, to 100000 s, with time. The variables and their ranges are given in Table 1. To cover all the range of input variables, the dataset was generated based on the design of the experiment (DOE). We generated the

Table 1
Simulation variables and their range of values for database generation.

Simulation variable	Range of values		Grid
Time (S)	10–1080000	10–3600	50
		3600–36000	500
		36000–360000	5000
		360000–1080000	100,000
Temperature (K)	850–970		10
Chromium composition	0.05–0.9		0.05
Cobalt composition	0.05–0.9		0.05

microstructures by solving the CH PDEs using the MOOSE framework [78] on Boise State University R2 cluster computers [80]. We note that because of the deterministic nature of the PF technique, i.e., not being stochastic, and the physics of the spinodal decomposition, we only need to run each condition once.

After simulations, we collected the morphology of Fe distribution, which represents the Fe-rich and Fe-depleted, i.e., Cr-rich, regions, as image data. In addition, we used the minimum and maximum compositions of Fe in each microstructure as numeric data. The deep network uses the image and numeric data as input to predict the time, temperature, and chemical compositions. Therefore, different types of deep networks like convolutional and fully-connected layers are required to process the input data.

We note that the accuracy of the model will increase for real materials if some experimental data is added to the training dataset. However, even having the experimental dataset to be just a few percent of the whole dataset, requires hundreds of tailored transmission electron microscopy (TEM) images. Generating such a big experimental dataset is time-consuming and costly. Therefore, in this work, we limit the model to synthetic data. However, as we will show in the validation part, Section 4, the model predicts the history of an experimental TEM image pretty well, because we are using a CALPHAD-informed phase field model to generate the training and test dataset and CALPHAD inherently is informed by some experimental data.

2.3. Deep learning methodology

Big data allows the use of deep neural networks for different applications like supervised learning, e.g., classification and regression tasks, and unsupervised learning, e.g., clustering [52,81]. Due to fused input data in this study, i.e., image and numeric data, two different layers, including convolutional and fully-connected layers, are needed to ingest the data. The image features are extracted through convolutional layers or transfer learning, and fully connected layers handle the numeric data. For transfer learning, we used the pretrained convolutional layers of the EfficientNet-B7 network for image feature extraction. After passing through a number of fully-connected layers, the numeric data will be combined with image extracted features by other fully-connected layers. The last layer will predict the time, temperature, and chemical compositions with four neurons with a linear activation function.

Two types of deep neural network layers are applied in the framework, fully-connected and convolutional layers. Fully-connected layers consist of neurons and activation functions [82] and convolutional layers use hidden layers consisting of convolutional, activation functions, pooling, and fully-connected layers that follow each other [52]. In the network configuration, the number of neurons is usually determined by trial and error. To enable the network to capture non-linear problems, the non-linearity is injected into the neural networks through the activation functions. There are several well-established activation functions such as linear, sigmoid, rectified linear (ReLU), leaky rectified linear, hyperbolic tangent (Tanh), Swish, and softmax that each of them is useful for specific applications [83]. Among all, the ReLU ($f(x) = \max(0, x)$) and Swish ($f(x) = x\,\mathrm{sigmoid}(x)$) have shown consistent robustness in a wide range of problems [84].

Using the convolutional neural networks (CNNs) for image processing and computer vision tasks was originally proposed by LeCun et al. [85]. CNNs have hidden layers consisting of convolutional, pooling, and fully-connected layers that follow each other. There are various types of CNNs based on the convolutional and pooling layers layout. Convolutional layers extract the salient features of images while the dimensionality of the data gets reduced through the fully-connected layers. In convolutional layers, a feature map is generated by passing filters over the images and scanning the pixel values. Then, the non-linearity property gets added to the system by passing the data through the activation function. The feature map size reduces by pooling operations, like maximum or average pooling, through the pooling layers. The image extracted features will be trained by adding fully-connected layers for specific tasks like classification, regression, and clustering. A cost function will train the CNN through the backpropagation. The number of filters, size, regularization values, dropout values, optimizer parameters, initial weights, and biases are updated during training. Since deep CNN training requires a large dataset, transfer learning is usually applied in many cases. In transfer learning, the target images, in our case, microstructure morphologies, are passed through a pretrained network that has been trained on the big image datasets such as ImageNet and can be used for another domain with domain adoption. Several pretrained net-

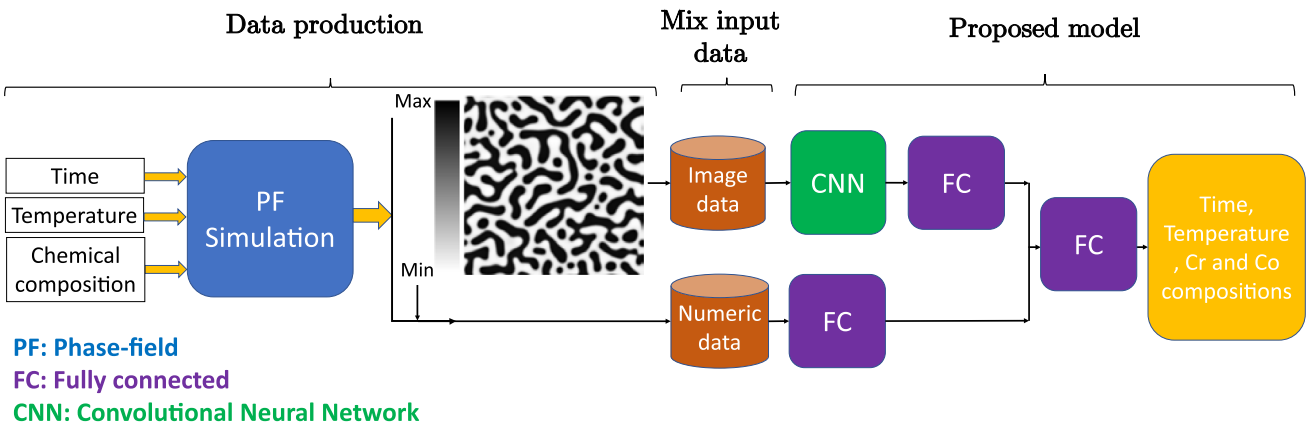

Fig. 2. The flowchart of the developed model for chemistry and processing history prediction from microstructure images (FC: fully-connected layer).

works have been used for materials microstructure quantification [26,66,68]. In this work, we will use the EfficientNet [86] network. Former study [75] demonstrated that convolutional layers of EfficientNet [86], as a fast and efficient pretrained network, can be applied for materials microstructures feature extraction. In this study, different in-house CNNs or different layers of pretrained convolutional layers of EfficientNet have been adopted to extract microstructures features.

PF simulations generate the training and test datasets in the framework. The proposed deep network in the framework includes different in-house CNNs or pretrained convolutional layers from EfficientNet-B7 (transfer learning) for microstructure feature extraction and fully-connected layers for processing of the extracted features and numeric data (iron minimum and maximum composition in the micrographs). CNNs with different convolutional layers are applied for microstructure feature extraction in the in-house CNNs. In transfer learning, different layers of pretrained convolutional network are tested to find the optimum number of layers based on the overall accuracy. The architecture of the proposed network is found by testing different combinations of convolutional, fully-connected layers and their parameters based on the best accuracy. A schematic flowchart of the proposed framework is given in Fig. 2. The extracted features of microstructures are passed through fully-connected layers to get combined with the output of the fully-connected layers that proceed the numeric data. The network is trained by the end-to-end method to find the optimum hyperparameters. The model parameters and specifications are listed in Table 2.

Table 2
Parameters selected for model specification, compilation, and cross-validation.

	Parameter	Selected value or option
Model Specification	Optimizer	Adam
	Learning Rate	1.00E-0.3
	Body activation	ReLU
	Output activation	Linear
	Input dimension	(224, 224, 1)
	Output dimension	(4)
Compilation	Loss	Mean absolute percentage error
	Optimizer	Adam
	Metric	Root Mean square error (RMSE), R squared
Cross-Validation	Fold	5
	Training data	80%
	Testing data	20%
	Batch size	8
	Epochs	750

3. Results and discussion

3.1. Phase-field modeling and dataset generation

We ran the PF model for the different combinations of time, temperature, and chemical compositions informed by the Simplex-Lattice design. Within the ranges given in Table 1, 125,233 different samples were simulated by the PF method, and the microstructures were extracted for different chemical compositions, temperatures, and time. Fig. 3 depicts the sample results of the PF simulation. MOOSE simulations of the 2D domains take approximately 120 service units (SU) per run on a 24 Core CPU. Therefore, screening the proposed range of different temperatures and chemical compositions for microstructure evolution required approximately 505 k SU to complete.

Since decomposition does not occur for all proposed operating conditions and chemistries, the microstructures showing the 0.1 difference in Fe composition between Cr-rich and Fe-rich phases and at least 15 % volume fraction for each phase were considered as spinodally decomposed results. Hence, only 14,376 samples in which decomposition has taken place are used to create the database. 80% of samples were used for training and 20% for testing. The training was validated by 5-fold cross-validation. The Fe-based composition microstructure morphologies, as well as minimum and maximum of Fe compositions in the microstructure along with corresponding time, temperature, and chemical compositions, form the dataset. A sample workflow of the dataset construction is given in Fig. 4.

3.2. Deep network training

First, the in-house CNNs with different convolutional layers have been tested to find the best architecture. The results are given in Table S2. The results indicate that the CNNs can predict the chemistry reasonably well. The accuracy of time prediction increases proportionally with the number of filters. However, the temperature accuracy is poor for all networks. According to previous study findings [75], the temperature is related to complicated microstructure features that can only be extracted by deep convolutional layers. Training such a deep network needs a very large training dataset, which is not available. Therefore, we adopted the transfer learning method to check the network accuracy. We used the EfficientNet-B7 convolutional layers to extract the salient

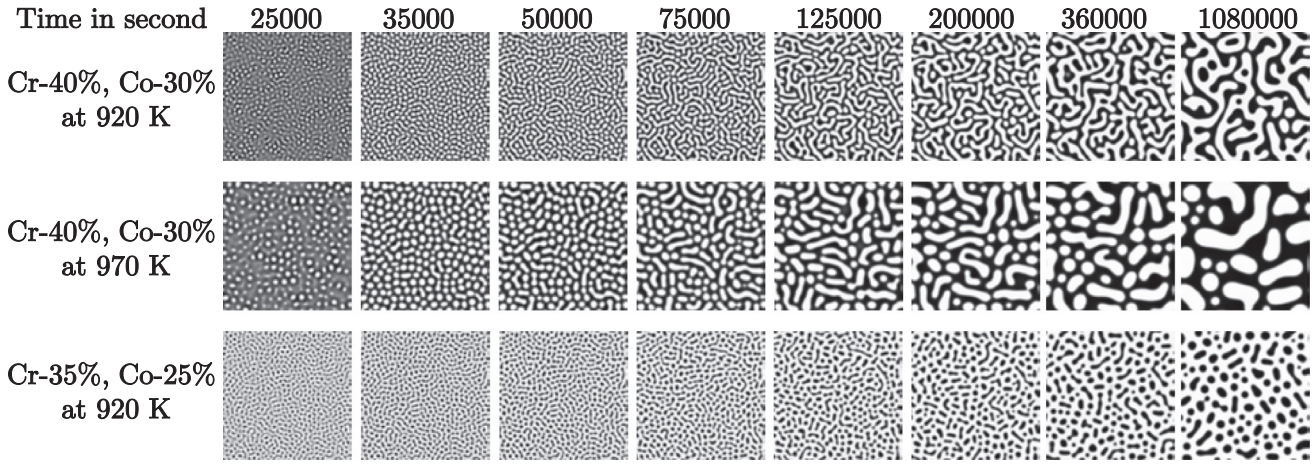

Fig. 3. The phase-field method generates Fe-Cr-Co alloy microstructures (Compositions are in atomic percent).

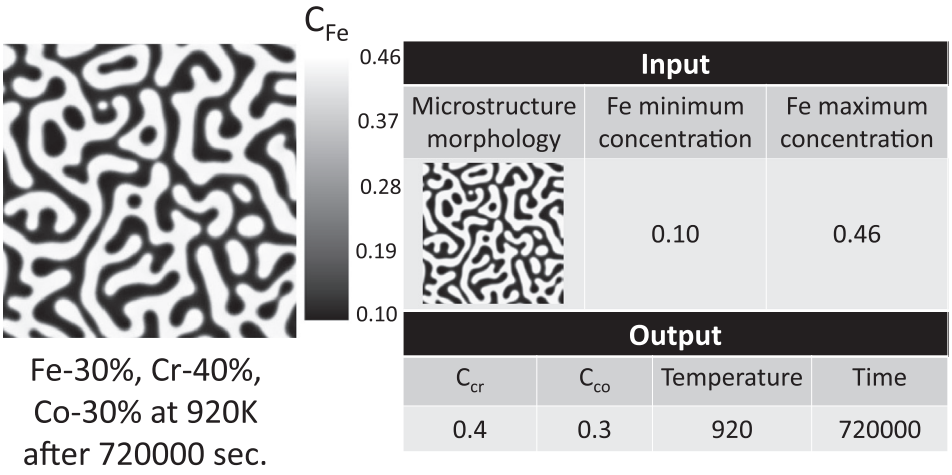

Fig. 4. A sample workflow of dataset construction.

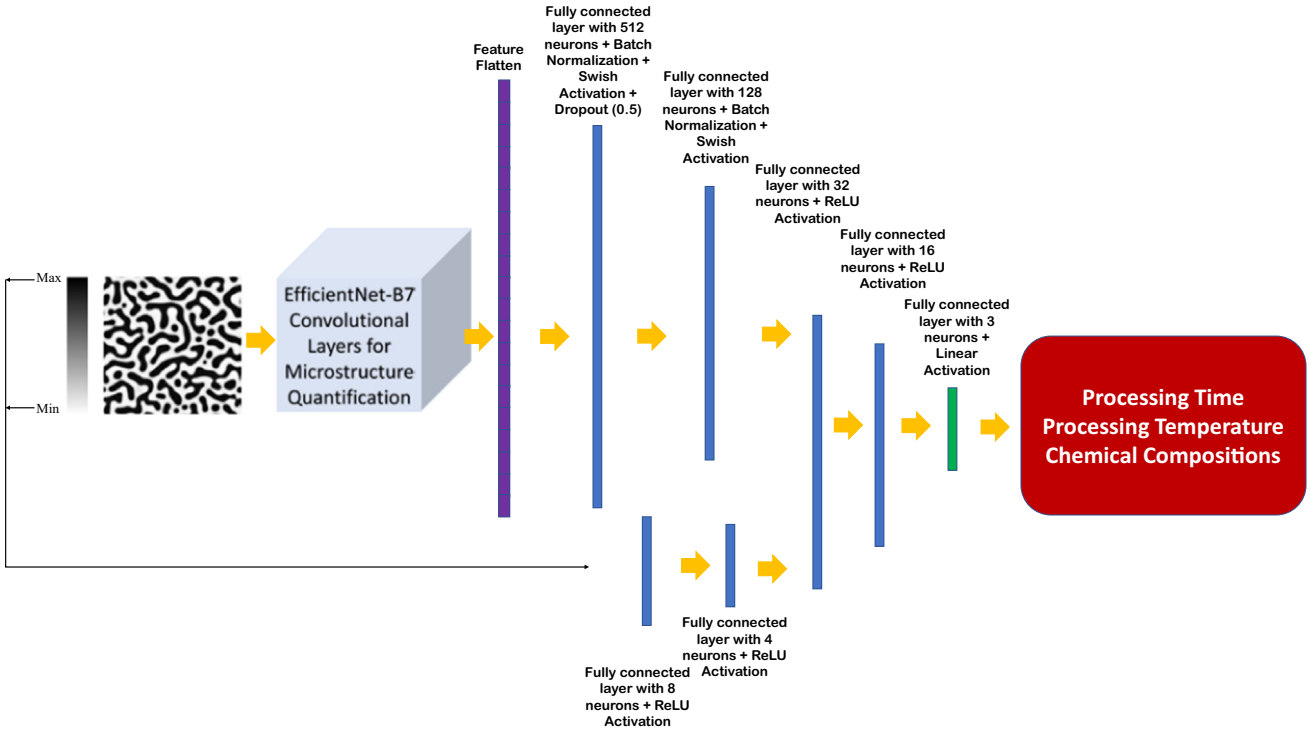

Fig. 5. The architecture of the proposed model (input image size is 224 × 224 pixels).

features of the produced microstructure by the PF method as transfer learning. The EfficientNet-B7 has 66 million parameters which are less than other networks with similar accuracies, such as VGG16, etc. Similar to other studies [87-89], the first layers capture simple features like edges, colors, and orientations. In contrast, the deeper layers extract more complicated, less visually interpretable features (see Fig. S1). The fused data, including microstructure morphology and Fe minimum and maximum concentration in morphology, are used for network training. Different pretrained convolutional layers of EfficientNet-B7 are applied to extract microstructures salient features while numeric data is proceeded by fully-connected layers. After passing fully-connected layers, the extracted features by convolutional layers are combined with the numeric data through the fully-connected layers to predict the outputs by linear activation function in the last layer, see Fig. 5. Convolutional layers 25, 108, 212, 286, 346, 406, 464, 509, 613, 673, 806, and 810 from EfficientNet-B7 are used to extract the microstructures features. For different convolutional layers, the model is trained based on the given parameters in Table 2. The model training is based on 5-fold cross-validation and dividing the dataset into training (80%) and testing (20%) datasets. The average R Squares and mean square error (MSE) for cross-validation and test set that the model never sees in the training process are given in Table S3. According to the results, the prediction of time and temperature is more challenging than compositions. Almost all the models can predict the compositions very well. The whole training process was repeated three times to check the models' stability. Finally, the most accurate prediction belongs to the model

that uses up to layer 286 of the EfficientNet-B7 for microstructures' quantification. The error distribution of this model, which shows a normal distribution, is given in Fig. S2.

In addition to cross-validation, testing data has also been used for overfitting detection. The training and validation losses diminish smoothly with epoch, as shown in Fig. 6a, and it is an indication that the model parameters converge to the global optimum without overfitting. A sample from the test set is given in Fig. 6b to show the developed model performance. The presented microstructure is for 15% Fe, 25% Cr, and 60% Co (all in atomic percent) after 195,000 s of heat treatment at 950 K. The model's predictions have good agreement with ground truth values for time, temperature, and chemical compositions. The parity plots with accuracy metrics for comparing the model prediction with ground truth for all testing data are shown in Fig. 6c. The results show that the model can predict the chemical compositions with the highest accuracy. The prediction accuracy for time and temperature is not as good as chemical compositions. But the model can still predict them reasonably well.

The results indicate that the time and temperature prediction is more challenging than chemical compositions, which is explainable by physical concepts. According to our simulation results (see Fig. S3) and reported studies [90,91], a slight change in initial chemical compositions can lead to a sensible change in microstructure morphology which is even recognizable by human eyes. Therefore, it will be uncomplicated for the model to realize the chemical composition changes. However, small changes in temperature will hardly lead to noticeable changes in the microstructure morphologies when the time and chemical composition are fixed. Therefore, finding these differences is hard and makes temperature prediction challenging. In the case of time, there are two different conditions. The morphology changes rapidly with time at the early stages of heat treatment, but the rate of change drops dramatically after some time, i.e., when the morphology reaches some stability, and changes will be minimal over time. This insensitivity will make the identification strenuous for the model. According to Table S3, the models can predict the chemical composition, temperature, and time in order of maximum to least accuracy. However, as we will discuss in the next section, most errors in time and temperatures, are not actually real errors, but just other right answers.

3.3. Model performance analysis

The R-square and RSME results for testing points show that the model can predict time, temperature, and chemical compositions well. However, the model's reliability depends on knowing the sources of the errors. Therefore, in this section, we will do a more in-depth study on some low-accuracy cases to find out the source of errors. As was mentioned earlier and according to the parity plots in Fig. 6c, the lowest accuracy belongs to time and temperature predictions. Some worst cases in time and temperature prediction are given in Fig. 7.

After studying some random cases, among the predictions with high errors, we concluded that two scenarios are possible for the sources of errors. One is achieving stability in the microstructure morphology after a certain time, and the second is achieving an identical microstructure from two different paths. Based on the observations and physical concepts, the microstructure morphologies change very sluggishly with time after passing the early stages of separation and coarsening, and reach some sort of stability. As mentioned earlier, once the stability is achieved, it is hard for the model to distinguish the differences between the microstructures due to the subtle or no changes between two considerable time steps. Therefore, we hypothesize that the errors that we observe in time predictions for high heat treatment times, i.e., times above 100 hrs, are associated with morphology stability. To test this

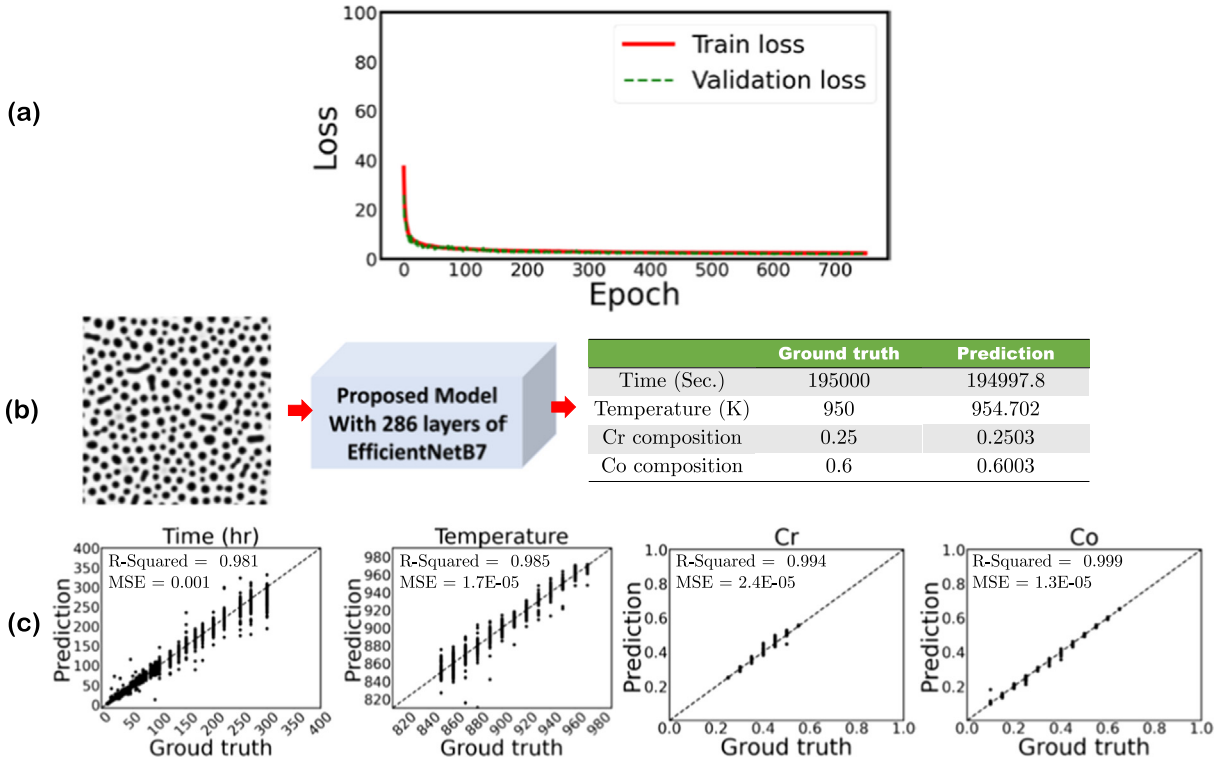

Fig. 6. a) Training and validation loss per each epoch, b) prediction of time, temperature, and chemical compositions for a random test dataset, and c) the parity plots for time, temperature, and chemical compositions for the testing dataset based on the transfer learning model when the first 286 layers of EfficientNetB7 are used for microstructures' feature extraction (The size of the input images are 224 × 224 pixels).

	Ground truth	Prediction	Ground truth	Prediction	Ground truth	Prediction	Ground truth	Prediction
Time (Sec.)	900000	1165722	1080000	844940.8	792000	1070176	1080000	920366.8
Temperature (K)	970	969.5409	950	950.3205	970	969.0656	910	910.8225
Cr composition	0.25	0.2505	0.4	0.4011	0.25	0.2509	0.5	0.4996
Co composition	0.45	0.4606	0.3	0.3006	0.35	0.3629	0.25	0.2482

	Ground truth	Prediction	Ground truth	Prediction	Ground truth	Prediction	Ground truth	Prediction
Time (Sec.)	900000	633511.2	1080000	815184.8	96000	107438.8	1080000	804410.9
Temperature (K)	850	863.4268	930	934.9607	880	863.9738	850	856.0246
Cr composition	0.3	0.2979	0.5	0.4966	0.4	0.4081	0.3	0.3074
Co composition	0.6	0.5999	0.1	0.1005	0.15	0.1482	0.55	0.543509

Fig. 7. Some worst cases for time (first row of images) and temperature (second row of images) predictions.

hypothesis, we compared the simulated microstructures based on the model's predictions with the microstructure given as the input, i.e., ground truth, to the modal. Quantitative comparison of different images can be made either by evaluating specific metrics or by observing the distribution of defined parameters in the images. We adopted some evaluation metrics that were widely used in the computer vision community including the Root Mean Squared Error (RMSE), Peak Signal-to-Noise Ratio (PSNR) [92,93], the Structural Similarity Index Measure (SSIM) [94], and the Learned Perceptual Image Patch Similarity (LPIPS) [95]. In these metrics, smaller RMSE and LPIPS, and higher PSNR and SSIM indicate more similarity between images. For distributions comparison between two images, two-point correlation function [96] and chord length [97] are standard techniques and we used them in this study. Fig. 8 shows the comparison between the ground truth and simulated microstructure for the first row of Fig. 7. We note that the simulated microstructures in Fig. 8 are informed by the DL-predicted chemistry, temperature, and time, i.e., the prediction values in Fig. 7. The evaluation metrics and distributions demonstrate that the two microstructures are similar, while there is about 70 hrs differences in their heat treatment times. These quantitative comparisons endorsed our hypothesis that the errors that we observe in time predictions for high heat treatment times are associated with the morphology stability.

Another source of error that we observed in predictions stems from the interplay between time and temperature. For these types of errors, we hypothesize that the predicted processing conditions, while being different from the ground truth, are indeed another path to reach a similar microstructure. To test this hypothesis, we ran the PF model with the predicted chemistry and processing parameters and compared quantitatively the simulated microstructures with the ground truth microstructures in Fig. 9. Again, the metrics and distributions show that the microstructures are very similar, and in fact, we can generate similar microstructures from two separate paths, i.e., higher time/lower temperature and lower time/higher temperature. Therefore, in these cases, the model does not predict wrong processing but just discovers a new path. Therefore, according to the model review results, the primary sources of errors, primarily in heat treatment time and temperature, root in the physical concepts behind the spinodal decomposition and are not inherently wrong predictions but just another right answer.

4. Validation of the proposed model with the experimental data

The main motivation of the proposed model is to enable the chemistry and processing history prediction of a micrograph. This makes the model a unique tool that enables, for the first-time, microstructure inverse design possible with no lost information, i.e., reducing the complexity of microstructure to just average grain size, etc. Since ultimately, the predicted chemistry and processing parameters are going to feed into the experiment, the model validation is crucial. In this section, we validate the model's predictability against an experimental transmission electron microscopy (TEM) image for spinodal decomposition of Fe-Cr-Co with the initial composition of 46% Fe, 31% Cr, and 23% Co after 100 hrs of heat treatment at 873 K from Okada et al. [91]. The original TEM image was larger than the model's required input size, so it was cropped to meet the 224x224 pixels size. Also, the Fe composition minimum and maximum in the micrograph were not given, and we selected these values by interpolating between the adjacent simulation points in the database. Fig. 10 shows the predictions of the model for the experimental TEM microstructure along with the ground truth.

Comparison between the predicted and ground truth shows that the model performs very well in terms of Co composition and temperature predictions with just 0.6% and 0.9% error, respectively. The predictions show 10% and 15% errors for annealing time and Cr composition, respectively. While all computational models naturally have some errors, we identify five key sources for the uncertainties in using the model for experimental micrographs, 1) the TEM micrograph does not have the image quality of the simulation microstructures, i.e., the training data, 2) the TEM image size was larger than the model's input, and we cropped it to 224x224 pixels, 3) the Fe composition was not reported for the TEM image and we used the PF input, 4) the model was trained with synthetic data and not TEM micrographs, 5) the PF model was parameterized with CALPHAD, and some errors correlate with uncertainty in CALPHAD data. These uncertainties can be reduced

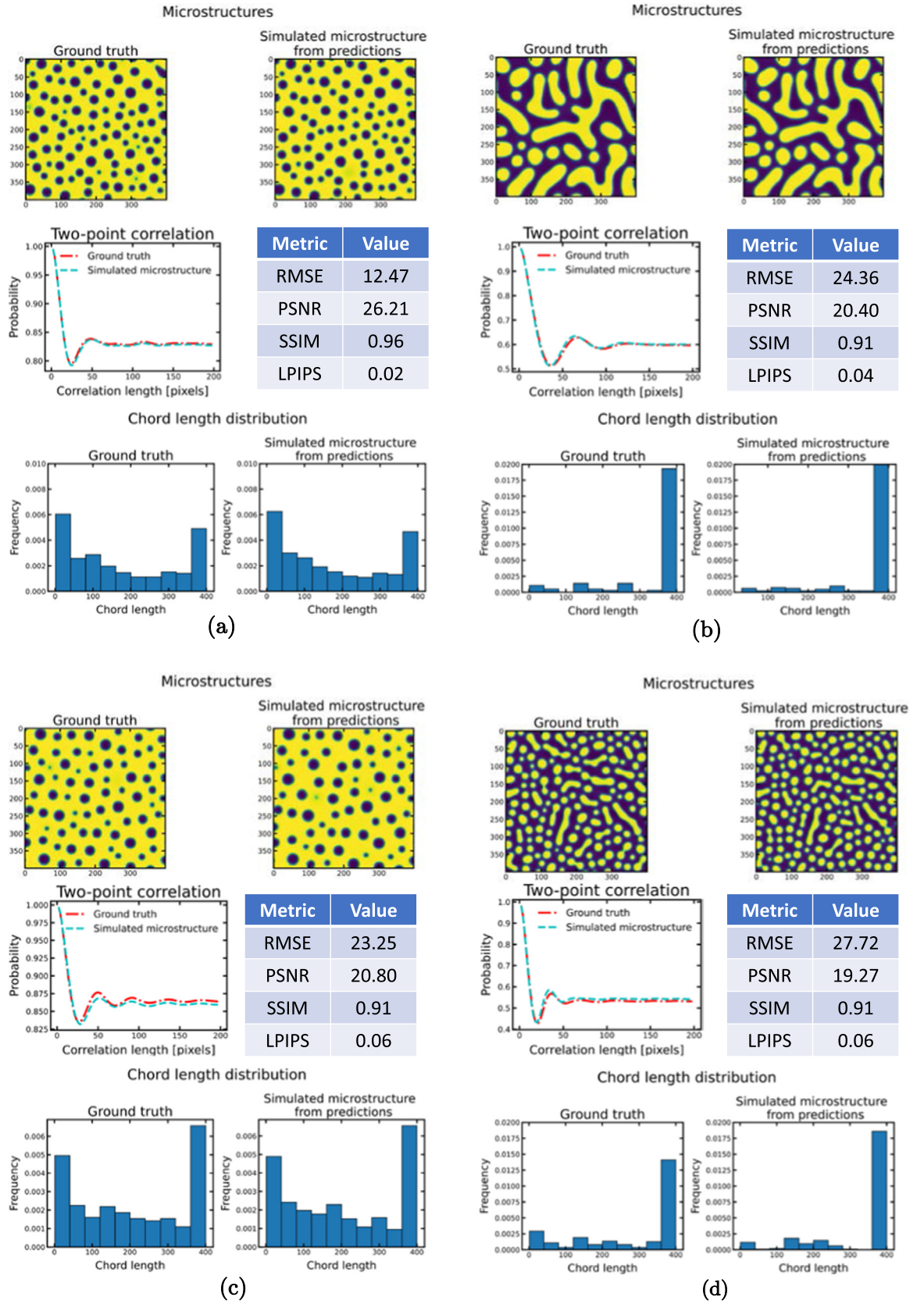

Metric	Value
RMSE	12.47
PSNR	26.21
SSIM	0.96
LPIPS	0.02

Metric	Value
RMSE	24.36
PSNR	20.40
SSIM	0.91
LPIPS	0.04

Metric	Value
RMSE	23.25
PSNR	20.80
SSIM	0.91
LPIPS	0.06

Metric	Value
RMSE	27.72
PSNR	19.27
SSIM	0.91
LPIPS	0.06

Fig. 8. Comparison of the ground truth microstructures with the simulated microstructures from model predictions for four random cases with high errors in time.

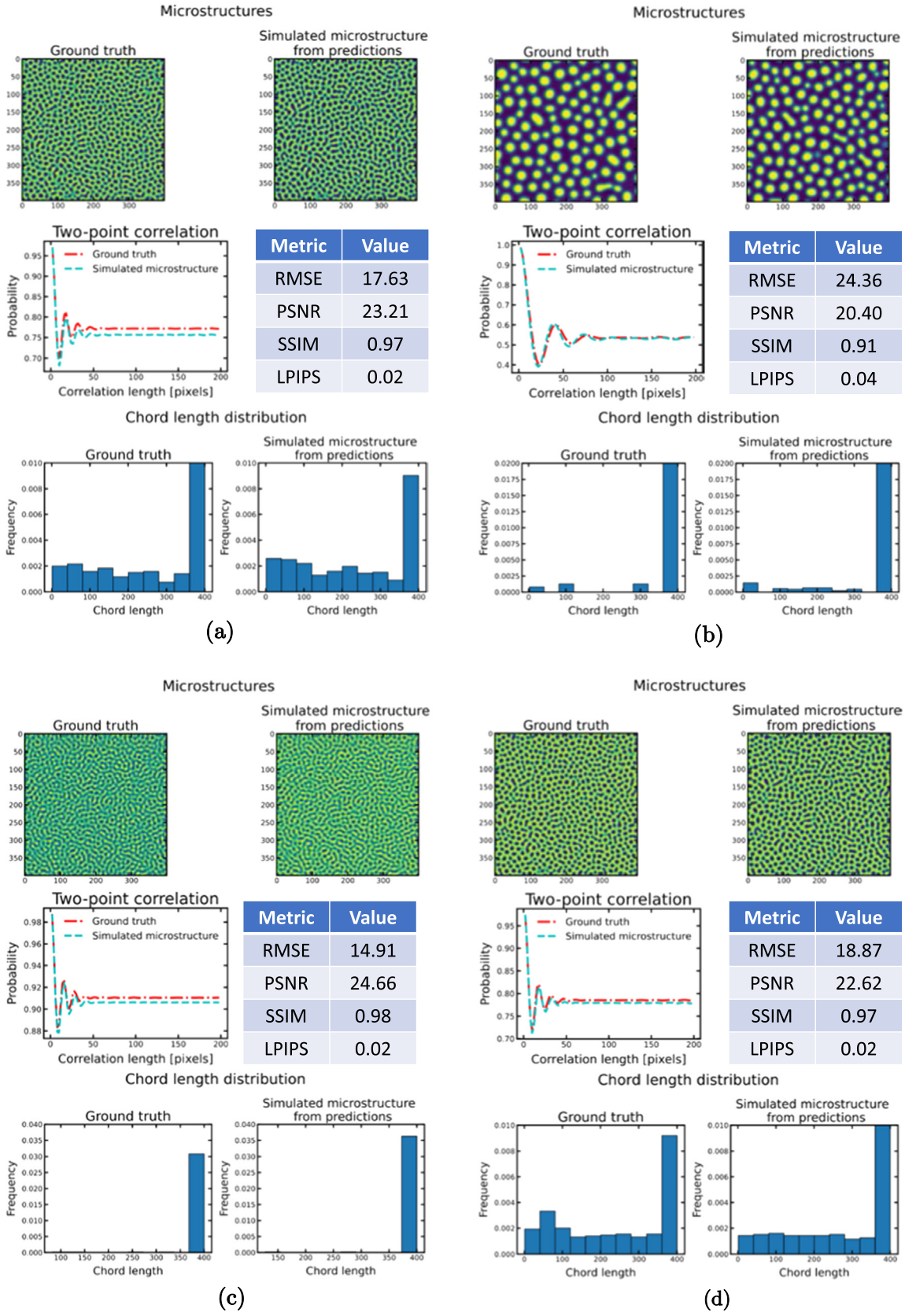

Metric	Value
RMSE	17.63
PSNR	23.21
SSIM	0.97
LPIPS	0.02

Metric	Value
RMSE	24.36
PSNR	20.40
SSIM	0.91
LPIPS	0.04

Metric	Value
RMSE	14.91
PSNR	24.66
SSIM	0.98
LPIPS	0.02

Metric	Value
RMSE	18.87
PSNR	22.62
SSIM	0.97
LPIPS	0.02

Fig. 9. Comparison of the ground truth microstructures with the simulated microstructures from model predictions for four random cases with errors in time and temperature.

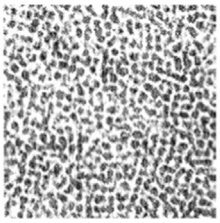

	Ground truth	Prediction
Time (Sec.)	360000	322020
Temperature (K)	873	881.904
Cr composition	0.31	0.3585
Co composition	0.23	0.2316

Fig. 10. Prediction of processing time, temperature, and chemistry for an experimental TEM image adopted from Okada et al. [91]. The original image was cropped to be in the desired size of 224 × 224 pixels.

if there are enough experimental images to be used in the training dataset. Despite all these shortcomings, the model's predictions for chemistry and processing history for the TEM micrograph were reasonably well.

5. Conclusion

In this work, we have developed a computational framework that enables the microstructure inverse design. As a model material, we studied the Fe-Cr-Co based permanent magnet alloys. The developed deep neural network is able to read a micrograph of one element distribution and predicts the chemistry and processing parameters that would lead to that micrograph. The model integrates the physics-based and data-driven modeling. The training and testing data were generated from the phase-field modeling of the spinodal decomposition process in Fe-Cr-Co alloys. The fused input data, including the microstructure morphologies and the associated minimum and maximum Fe composition, were used to train the proposed network to predict the heat treatment time and temperature as well as the initial chemical composition, i.e., the Cr and Co. We used different CNN layers as well as different convolutional layers of EfficientNet-B7 pretrained networks to quantify the microstructure morphologies. The accuracy metrics, parity plots, and error distribution demonstrate that the model with the EfficientNet-B7 pretrained network performs well on the training data. We found that temperature is the most challenging parameter to predict and it requires deeper layers and more complicated extracted features from microstructures. The error analysis showed that some wrong predictions, in particular the ones with high errors in time and temperature predictions, are not actually wrong but just other correct answers. We identified that the errors are associated with either the microstructure morphology stability or the possibility of having one microstructure with two processing paths. Finally, we validated the model with an experimental TEM microstructure and the model was able to predict the processing history and chemistry of the TEM micrograph reasonably well. The process parameters and chemistry prediction for experimental micrographs can improve significantly if we have the right size, and high-resolution microstructures, and also add some experimental data to the training dataset.

6. Data availability

The raw/processed data and codes required to reproduce these findings are available at https://github.com/Amir1361/time_temperature_composition_predictionhttps://github.com/Amir1361/Materials_Design_by_ML_DL.

CRediT authorship contribution statement

Amir Abbas Kazemzadeh Farizhandi: Conceptualization, Investigation, Methodology, Software, Writing – original draft, Date curation, Formal Analysis, Validation, Visualization. **Mahmood Mamivand:** Conceptualization, Investigation, Data curation, Supervision, Funding acquisition.

Declaration of Competing Interest

The authors declare the following financial interests/personal relationships which may be considered as potential competing interests: Mahmood Mamivand reports financial support was provided by National Science Foundation.

Acknowledgement

The authors appreciate the support of Boise State University. This work was supported in part by the National Science Foundation grant DMR-2142935. We also would like to acknowledge the high-performance computing support of the R2 compute cluster (DOI: 10.18122/B2S41H) and the Borah compute cluster (DOI: 10.18122/oit/3/boisestate) provided by Boise State University's Research Computing Department. This work also used the Extreme Science and Engineering Discovery Environment (XSEDE), which is supported by the National Science Foundation grant number ACI-1548562.

Appendix A. Supplementary data

Supplementary data to this article can be found online at https://doi.org/10.1016/j.matdes.2022.110799.

References

[1] L. Himanen, A. Geurts, A.S. Foster, P. Rinke, Data-Driven Materials Science: Status, Challenges, and Perspectives, Adv. Sci. 6 (21) (2019) 1900808, https://doi.org/10.1002/advs.201900808.
[2] J. Schmidt, M.R.G. Marques, S. Botti, M.A.L. Marques, Recent advances and applications of machine learning in solid-state materials science, npj Comput Mater 5 (1) (2019), https://doi.org/10.1038/s41524-019-0221-0.
[3] R. Pollice, G. dos Passos Gomes, M. Aldeghi, R.J. Hickman, M. Krenn, C. Lavigne, M. Lindner-D'Addario, AkshatKumar Nigam, C.T. Ser, Z. Yao, A. Aspuru-Guzik, Data-Driven Strategies for Accelerated Materials Design, Acc. Chem. Res. 54 (4) (2021) 849–860, https://doi.org/10.1021/acs.accounts.0c00785.
[4] T. Zhou, Z. Song, K. Sundmacher, Big data creates new opportunities for materials research: A review on methods and applications of machine learning for materials design, Engineering 5 (6) (2019) 1017–1026, https://doi.org/10.1016/j.eng.2019.02.011.
[5] D.L. McDowell, S.R. Kalidindi, The materials innovation ecosystem: A key enabler for the Materials Genome Initiative, MRS Bull. 41 (4) (2016) 326–337, https://doi.org/10.1557/mrs.2016.61.
[6] Materials Genome Initiative https://www.mgi.gov.
[7] E. van der Giessen, P.A. Schultz, N. Bertin, V.V. Bulatov, W. Cai, G. Csányi, S.M. Foiles, M.G.D. Geers, C. González, M. Hütter, W.K. Kim, D.M. Kochmann, J. LLorca, A.E. Mattsson, J. Rottler, A. Shluger, R.B. Sills, I. Steinbach, A. Strachan, E. B. Tadmor, Roadmap on multi-scale materials modeling, Modell. Simul. Mater. Sci. Eng. 28 (4) (2020) 043001.
[8] X. Liu, D. Furrer, J. Kosters, J. Holmes, Vision 2040: a roadmap for integrated, multi-scale modeling and simulation of materials and systems, 2018.
[9] M. Vassaux, R.C. Sinclair, R.A. Richardson, J.L. Suter, P.V. Coveney, Toward High Fidelity Materials Property Prediction from Multi-scale Modeling and Simulation, Adv. Theory Simulations 3 (1) (2020) 1900122, https://doi.org/10.1002/adts.201900122.
[10] J. Bi, et al., Multi-scale modeling for the science and engineering of materials, 19, 1–80, doi:10.1615/IntJMultCompEng.2021040247 (2021).

[11] K. Matouš, M.G.D. Geers, V.G. Kouznetsova, A. Gillman, A review of predictive non-linear theories for multi-scale modeling of heterogeneous materials, J. Comput. Phys. 330 (2017) 192–220, https://doi.org/10.1016/j.jcp.2016.10.070.
[12] S.R. Kalidindi, D.B. Brough, S. Li, A. Cecen, A.L. Blekh, F.Y.P. Congo, C. Campbell, Role of materials data science and informatics in accelerated materials innovation, MRS Bull. 41 (08) (2016) 596–602, https://doi.org/10.1557/mrs.2016.164.
[13] P.M. Voyles, Informatics and data science in materials microscopy, Curr. Opin. Solid State Mater. Sci. 21 (3) (2017) 141–158, https://doi.org/10.1016/j.cossms.2016.10.001.
[14] M. Haghighatlari, G. Vishwakarma, D. Altarawy, R. Subramanian, B.U. Kota, A. Sonpal, S. Setlur, J. Hachmann, ChemML: A machine learning and informatics program package for the analysis, mining, and modeling of chemical and materials data, WIREs Comput. Mol. Sci. 10 (4) (2020), https://doi.org/10.1002/wcms.1458.
[15] S.R. Kalidindi, M. De Graef, Materials Data Science: Current Status and Future Outlook, Annu. Rev. Mater. Res. 45 (1) (2015) 171–193, https://doi.org/10.1146/annurev-matsci-070214-020844.
[16] T.J. Oweida, A. Mahmood, M.D. Manning, S. Rigin, Y.G. Yingling, Merging Materials and Data Science: Opportunities, Challenges, and Education in Materials Informatics, MRS Adv. 5 (7) (2020) 329–346, https://doi.org/10.1557/adv.2020.171.
[17] S.R. Kalidindi, A.J. Medford, D.L. McDowell, Vision for Data and Informatics in the Future Materials Innovation Ecosystem, JOM 68 (8) (2016) 2126–2137, https://doi.org/10.1007/s11837-016-2036-5.
[18] S. Ramakrishna, T.-Y. Zhang, W.-C. Lu, Q. Qian, J.S.C. Low, J.H.R. Yune, D.Z.L. Tan, S. Bressan, S. Sanvito, S.R. Kalidindi, Materials informatics, J. Intell. Manuf. 30 (6) (2019) 2307–2326, https://doi.org/10.1007/s10845-018-1392-0.
[19] A. Khosravani, A. Cecen, S.R. Kalidindi, Development of high throughput assays for establishing process-structure-property linkages in multiphase polycrystalline metals: Application to dual-phase steels, Acta Mater. 123 (2017) 55–69, https://doi.org/10.1016/j.actamat.2016.10.033.
[20] A. Cecen, H. Dai, Y.C. Yabansu, S.R. Kalidindi, L. Song, Material structure-property linkages using three-dimensional convolutional neural networks, Acta Mater. 146 (2018) 76–84, https://doi.org/10.1016/j.actamat.2017.11.053.
[21] J. Jung, J.I. Yoon, H.K. Park, J.Y. Kim, H.S. Kim, An efficient machine learning approach to establish structure-property linkages, Comput. Mater. Sci. 156 (2019) 17–25, https://doi.org/10.1016/j.commatsci.2018.09.034.
[22] D.B. Brough, D. Wheeler, J.A. Warren, S.R. Kalidindi, Microstructure-based knowledge systems for capturing process-structure evolution linkages, Curr. Opin. Solid State Mater. Sci. 21 (3) (2017) 129–140, https://doi.org/10.1016/j.cossms.2016.05.002.
[23] G. Whelan, D.L. McDowell, Machine Learning-Enabled Uncertainty Quantification for Modeling Structure-Property Linkages for Fatigue Critical Engineering Alloys Using an ICME Workflow, Integr. Mater. Manuf. Innov. 9 (4) (2020) 376–393, https://doi.org/10.1007/s40192-020-00192-2.
[24] Y.C. Yabansu, P. Steinmetz, J. Hötzer, S.R. Kalidindi, B. Nestler, Extraction of reduced-order process-structure linkages from phase-field simulations, Acta Mater. 124 (2017) 182–194, https://doi.org/10.1016/j.actamat.2016.10.071.
[25] B. Meredig, Five High-Impact Research Areas in Machine Learning for Materials Science, Chem. Mater. 31 (23) (2019) 9579–9581, https://doi.org/10.1021/acs.chemmater.9b04078.
[26] J. Ling, M. Hutchinson, E. Antono, B. DeCost, E.A. Holm, B. Meredig, Building data-driven models with microstructural images: Generalization and interpretability, Mater. Discover 10 (2017) 19–28, https://doi.org/10.1016/j.md.2018.03.002.
[27] A.A.K. Farizhandi, H. Zhao, R. Lau, Modeling the change in particle size distribution in a gas-solid fluidized bed due to particle attrition using a hybrid artificial neural network-genetic algorithm approach, Chem. Eng. Sci. 155 (2016) 210–220.
[28] A.A.K. Farizhandi, H. Zhao, T. Chen, R. Lau, Evaluation of material properties using planetary ball milling for modeling the change of particle size distribution in a gas-solid fluidized bed using a hybrid artificial neural network-genetic algorithm approach, Chem. Eng. Sci. 215 (2020) 115469, https://doi.org/10.1016/j.ces.2020.115469.
[29] A.A.K. Farizhandi, A. Pacławski, J. Szlęk, A. Mendyk, Y.-H. Shao, R. Lau, Evaluation of carrier size and surface morphology in carrier-based dry powder inhalation by surrogate modeling, Chem. Eng. Sci. 193 (2019) 144–155, https://doi.org/10.1016/j.ces.2018.09.007.
[30] K. Farizhandi, A. Abbas, Surrogate modeling applications in chemical and biomedical processes, Doctor of Philosophy thesis, Nanyang Technological University, 2017.
[31] A.A.K. Farizhandi, M. Alishiri, R. Lau, Machine learning approach for carrier surface design in carrier-based dry powder inhalation, Comput. Chem. Eng. 151 (2021) 107367, https://doi.org/10.1016/j.compchemeng.2021.107367.
[32] L. Li et al., Understanding machine-learned density functionals, Int. J. Quantum Chem. 116 (2016) 819–833, https://doi.org/10.1002/qua.25040.
[33] R. Nagai, R. Akashi, O. Sugino, Completing density functional theory by machine learning hidden messages from molecules, npj Comput Mater 6 (1) (2020), https://doi.org/10.1038/s41524-020-0310-0.
[34] J.C. Snyder, M. Rupp, K. Hansen, K.-R. Müller, K. Burke, Finding density functionals with machine learning, Phys. Rev. Lett. 108 (2012), https://doi.org/10.1103/PhysRevLett.108.253002 253002.
[35] J.E. Gubernatis, T. Lookman, Machine learning in materials design and discovery: Examples from the present and suggestions for the future, Phys. Rev. Mater. 2 (2018), https://doi.org/10.1103/PhysRevMaterials.2.120301 120301.
[36] D.B. Brough, D. Wheeler, S.R. Kalidindi, Materials Knowledge Systems in Python—a Data Science Framework for Accelerated Development of Hierarchical Materials, Integr. Mater. Manuf. Innov. 6 (1) (2017) 36–53, https://doi.org/10.1007/s40192-017-0089-0.
[37] E. Kautz, W. Ma, S. Jana, A. Devaraj, V. Joshi, B. Yener, D. Lewis, An image-driven machine learning approach to kinetic modeling of a discontinuous precipitation reaction, Mater. Charact. 166 (2020) 110379, https://doi.org/10.1016/j.matchar.2020.110379.
[38] R. Bostanabad, Y. Zhang, X. Li, T. Kearney, L.C. Brinson, D.W. Apley, W.K. Liu, W. Chen, Computational microstructure characterization and reconstruction: Review of the state-of-the-art techniques, Prog. Mater Sci. 95 (2018) 1–41, https://doi.org/10.1016/j.pmatsci.2018.01.005.
[39] A. Agrawal, A. Choudhary, Deep materials informatics: Applications of deep learning in materials science, MRS Commun. 9 (3) (2019) 779–792, https://doi.org/10.1557/mrc.2019.73.
[40] D. Jha, L. Ward, A. Paul, W.-K. Liao, A. Choudhary, C. Wolverton, A. Agrawal, Elemnet: Deep learning the chemistry of materials from only elemental composition, Sci. Rep. 8 (1) (2018), https://doi.org/10.1038/s41598-018-35934-y.
[41] D. Xue, D. Xue, R. Yuan, Y. Zhou, P.V. Balachandran, X. Ding, J. Sun, T. Lookman, An informatics approach to transformation temperatures of NiTi-based shape memory alloys, Acta Mater. 125 (2017) 532–541.
[42] B. Meredig, E. Antono, C. Church, M. Hutchinson, J. Ling, S. Paradiso, B. Blaiszik, I. Foster, B. Gibbons, J. Hattrick-Simpers, A. Mehta, L. Ward, Can machine learning identify the next high-temperature superconductor? Examining extrapolation performance for materials discovery, Mol. Syst. Des. Eng. 3 (5) (2018) 819–825.
[43] B. Meredig, A. Agrawal, S. Kirklin, J.E. Saal, J.W. Doak, A. Thompson, K. Zhang, A. Choudhary, C. Wolverton, Combinatorial screening for new materials in unconstrained composition space with machine learning, Phys. Rev. B 89 (9) (2014), https://doi.org/10.1103/PhysRevB.89.094104.
[44] G.H. Teichert, K. Garikipati, Machine learning materials physics: Surrogate optimization and multi-fidelity algorithms predict precipitate morphology in an alternative to phase field dynamics, Comput. Methods Appl. Mech. Eng. 344 (2019) 666–693.
[45] E. Popova, T.M. Rodgers, X. Gong, A. Cecen, J.D. Madison, S.R. Kalidindi, Process-Structure Linkages Using a Data Science Approach: Application to Simulated Additive Manufacturing Data, Integr. Mater. Manuf. Innov. 6 (1) (2017) 54–68, https://doi.org/10.1007/s40192-017-0088-1.
[46] M.I. Latypov, M. Kühbach, I.J. Beyerlein, J.-C. Stinville, L.S. Toth, T.M. Pollock, S. R. Kalidindi, Application of chord length distributions and principal component analysis for quantification and representation of diverse polycrystalline microstructures, Mater. Charact. 145 (2018) 671–685, https://doi.org/10.1016/j.matchar.2018.09.020.
[47] G. Pilania, C. Wang, X. Jiang, S. Rajasekaran, R. Ramprasad, Accelerating materials property predictions using machine learning, Sci. Rep. 3 (2013) 1–6.
[48] Z. Del Rosario, M. Rupp, Y. Kim, E. Antono, J. Ling, Assessing the frontier: Active learning, model accuracy, and multi-objective candidate discovery and optimization, J. Chem. Phys. 153 (2020) 024112.
[49] D. Jha, K. Choudhary, F. Tavazza, W.-K. Liao, A. Choudhary, C. Campbell, A. Agrawal, Enhancing materials property prediction by leveraging computational and experimental data using deep transfer learning, Nat. Commun. 10 (1) (2019), https://doi.org/10.1038/s41467-019-13297-w.
[50] Y. Chen, S. Duffner, A. Stoian, J.-Y. Dufour, A. Baskurt, Deep and low-level feature based attribute learning for person re-identification, Image Vis. Comput. 79 (2018) 25–34, https://doi.org/10.1016/j.imavis.2018.09.001.
[51] G.E. Hinton, To recognize shapes, first learn to generate images, Prog. Brain Res. 165 (2007) 535–547.
[52] Y. LeCun, Y. Bengio, G. Hinton, Deep learning, Nature 521 (7553) (2015) 436–444.
[53] D. Amodei, et al., Deep Speech 2 : End-to-End Speech Recognition in English and Mandarin, in: International conference on machine learning, 173-182.
[54] R. Cang, Y. Xu, S. Chen, Y. Liu, Y. Jiao, M. Yi Ren, Microstructure representation and reconstruction of heterogeneous materials via deep belief network for computational material design, J. Mech. Des. 139 (7) (2017), https://doi.org/10.1115/1.4036649.
[55] B.L. DeCost, B.o. Lei, T. Francis, E.A. Holm, High throughput quantitative metallography for complex microstructures using deep learning: a case study in ultrahigh carbon steel, Microsc. Microanal. 25 (1) (2019) 21–29.
[56] T. Xie, J.C. Grossman, Crystal graph convolutional neural networks for an accurate and interpretable prediction of material properties, Phys. Rev. Lett. 120 (14) (2018), https://doi.org/10.1103/PhysRevLett.120.145301.
[57] K. Ryan, J. Lengyel, M. Shatruk, Crystal Structure Prediction via Deep Learning, J. Am. Chem. Soc. 140 (32) (2018) 10158–10168, https://doi.org/10.1021/jacs.8b0391310.1021/jacs.8b03913.s00110.1021/jacs.8b03913.s002.
[58] Z. Yang, Y.C. Yabansu, R. Al-Bahrani, W.-K. Liao, A.N. Choudhary, S.R. Kalidindi, A. Agrawal, Deep learning approaches for mining structure-property linkages in high contrast composites from simulation datasets, Comput. Mater. Sci. 151 (2018) 278–287, https://doi.org/10.1016/j.commatsci.2018.05.014.
[59] G. Landi, S.R. Niezgoda, S.R. Kalidindi, Multi-scale modeling of elastic response of three-dimensional voxel-based microstructure datasets using novel DFT-based knowledge systems, Acta Mater. 58 (7) (2010) 2716–2725.

[60] S.R. Kalidindi, S.R. Niezgoda, G. Landi, S. Vachhani, T. Fast, A novel framework for building materials knowledge systems, Comput., Mater., Continua 17 (2010) 103–125.
[61] T. Fast, S.R. Kalidindi, Formulation and calibration of higher-order elastic localization relationships using the MKS approach, Acta Mater. 59 (11) (2011) 4595–4605.
[62] Z. Yang, Y.C. Yabansu, D. Jha, W.-K. Liao, A.N. Choudhary, S.R. Kalidindi, A. Agrawal, Establishing structure-property localization linkages for elastic deformation of three-dimensional high contrast composites using deep learning approaches, Acta Mater. 166 (2019) 335–345, https://doi.org/10.1016/j.actamat.2018.12.045.
[63] R. Liu, Y.C. Yabansu, A. Agrawal, S.R. Kalidindi, A.N. Choudhary, Machine learning approaches for elastic localization linkages in high-contrast composite materials, Integr. Mater. Manuf. Innov. 4 (1) (2015) 192–208, https://doi.org/10.1186/s40192-015-0042-z.
[64] R. Liu, Y.C. Yabansu, Z. Yang, A.N. Choudhary, S.R. Kalidindi, A. Agrawal, Context Aware Machine Learning Approaches for Modeling Elastic Localization in Three-Dimensional Composite Microstructures, Integr. Mater. Manuf. Innov. 6 (2) (2017) 160–171, https://doi.org/10.1007/s40192-017-0094-3.
[65] J. Deng, et al., in: 2009 IEEE Conference on Computer Vision and Pattern Recognition, 248–255.
[66] B.L. DeCost, T. Francis, E.A. Holm, Exploring the microstructure manifold: image texture representations applied to ultrahigh carbon steel microstructures, Acta Mater. 133 (2017) 30–40.
[67] N. Lubbers, T. Lookman, K. Barros, Inferring low-dimensional microstructure representations using convolutional neural networks, Phys. Rev. E 96 (5) (2017), https://doi.org/10.1103/PhysRevE.96.052111.
[68] X. Li et al., A transfer learning approach for microstructure reconstruction and structure-property predictions, Sci. Rep. 8 (2018) 1–13.
[69] R. Cohn, E. Holm, Unsupervised Machine Learning Via Transfer Learning and k-Means Clustering to Classify Materials Image Data, Integr. Mater. Manuf. Innov. 10 (2) (2021) 231–244, https://doi.org/10.1007/s40192-021-00205-8.
[70] O. Russakovsky, J. Deng, H. Su, J. Krause, S. Satheesh, S. Ma, Z. Huang, A. Karpathy, A. Khosla, M. Bernstein, A.C. Berg, L.i. Fei-Fei, Imagenet large scale visual recognition challenge, Int. J. Comput. Vision 115 (3) (2015) 211–252.
[71] Q. Luo, E.A. Holm, C. Wang, A transfer learning approach for improved classification of carbon nanomaterials from TEM images, Nanoscale Adv. 3 (1) (2021) 206–213, https://doi.org/10.1039/D0NA00634C.
[72] A. Chowdhury, E. Kautz, B. Yener, D. Lewis, Image driven machine learning methods for microstructure recognition, Comput. Mater. Sci. 123 (2016) 176–187, https://doi.org/10.1016/j.commatsci.2016.05.034.
[73] R. Bostanabad, Reconstruction of 3D Microstructures from 2D Images via Transfer Learning, Comput. Aided Des. 128 (2020) 102906, https://doi.org/10.1016/j.cad.2020.102906.
[74] W. Ma, E.J. Kautz, A. Baskaran, A. Chowdhury, V. Joshi, B. Yener, D.J. Lewis, Image-driven discriminative and generative machine learning algorithms for establishing microstructure–processing relationships, J. Appl. Phys. 128 (13) (2020) 134901, https://doi.org/10.1063/5.0013720.
[75] F. Amir Abbas Kazemzadeh, B. Omar, M. Mahmood, Deep Learning Approach for Chemistry and Processing History Prediction from Materials Microstructure, Scientific Reports, doi:10.21203/rs.3.rs-953170/v1 (2021).
[76] M. de Oca, D. Zapiain, J.A. Stewart, R. Dingreville, Accelerating phase-field-based microstructure evolution predictions via surrogate models trained by machine learning methods, npj Comput. Mater. 7 (2021) 1–11.
[77] T. Koyama, H. Onodera, Phase-Field simulation of phase decomposition in Fe–Cr– Co alloy under an external magnetic field, Met. Mater. Int. 10 (4) (2004) 321–326.
[78] C.J. Permann, D.R. Gaston, D. Andrš, R.W. Carlsen, F. Kong, A.D. Lindsay, J.M. Miller, J.W. Peterson, A.E. Slaughter, R.H. Stogner, R.C. Martineau, MOOSE: Enabling massively parallel multiphysics simulation, SoftwareX 11 (2020) 100430, https://doi.org/10.1016/j.softx.2020.100430.
[79] J.A. Cornell, Experiments with Mixtures: A Review, Technometrics 15 (3) (1973) 437–455, https://doi.org/10.1080/00401706.1973.10489071.
[80] Department. Boise State's Research Computing, R2: Dell HPC Intel E5v4 (High Performance Computing Cluster), Boise State University, Boise, ID, 2017, https://doi.org/10.18122/B2S41H.
[81] H. Wang, B. Raj, On the origin of deep learning, *arXiv preprint arXiv:1702.07800,* 2017.
[82] M.A. Nielsen, Neural networks and deep learning, Vol. 25, Determination press, 2015.
[83] C. Nwankpa, W. Ijomah, A. Gachagan, S. Marshall, Activation functions: Comparison of trends in practice and research for deep learning, *arXiv preprint arXiv:1811.03378,* 2018.
[84] T. Szandała, Review and Comparison of Commonly Used Activation Functions for Deep Neural Networks., Bio-inspired Neurocomputing, Springer, 2021, pp. 203–224.
[85] Y. Lecun, L. Bottou, Y. Bengio, P. Haffner, Gradient-based learning applied to document recognition, Proc. IEEE 86 (1998) 2278–2324, https://doi.org/10.1109/5.726791.
[86] M. Tan, Q.V. Le, Efficientnet: Rethinking model scaling for convolutional neural networks, *arXiv preprint arXiv:1905.11946,* 2019.
[87] C. Szegedy, V. Vanhoucke, S. Ioffe, J. Shlens, Z. Wojna, in: Proceedings of the IEEE conference on computer vision and pattern recognition, 2818–2826.
[88] F. Chollet, in: Proceedings of the IEEE conference on computer vision and pattern recognition, 1251–1258.
[89] F. Chollet, Deep learning with Python, Vol. 361, Manning, 2018.
[90] T. Koyama, H. Onodera, Phase-Field simulation of phase decomposition in Fe−Cr−Co alloy under an external magnetic field, Met. Mater. Int. 10 (4) (2004) 321–326, https://doi.org/10.1007/BF03185980.
[91] M. Okada, G. Thomas, M. Homma, H. Kaneko, Microstructure and magnetic properties of Fe-Cr-Co alloys, IEEE Trans. Magn. 14 (4) (1978) 245–252.
[92] J.-B. Martens, L. Meesters, Image dissimilarity, Signal Process. 70 (3) (1998) 155–176, https://doi.org/10.1016/S0165-1684(98)00123-6.
[93] A.M. Eskicioglu, P.S. Fisher, Image quality measures and their performance, IEEE Trans. Commun. 43 (1995) 2959–2965, https://doi.org/10.1109/26.477498.
[94] Z. Wang, A.C. Bovik, H.R. Sheikh, E.P. Simoncelli, Image quality assessment: from error visibility to structural similarity, IEEE Trans. Image Process. 13 (4) (2004) 600–612, https://doi.org/10.1109/TIP.2003.819861.
[95] R. Zhang, P. Isola, A.A. Efros, E. Shechtman, O. Wang, in: Proceedings of the IEEE conference on computer vision and pattern recognition, 586-595.
[96] M. Kerscher, I. Szapudi, A.S. Szalay, A Comparison of Estimators for the Two-Point Correlation Function, Astrophys. J. 535 (2000) L13–L16, https://doi.org/10.1086/312702.
[97] W. Gille, Chord length distributions and small-angle scattering, Eur. Phys. J. B - Condensed Matter Complex Syst. 17 (3) (2000) 371–383, https://doi.org/10.1007/s100510070116.